EPR Studies of 1:1 Complexes of Rhodium(II) and Cobalt(II) Porphyrins with σ Donor and π Acceptor Ligands: Origins of Rhodium(II) Metalloradical Reactivity

Bradford B. Wayland,* Alan E. Sherry, and Andrew G. Bunn

Contribution from the Department of Chemistry, University of Pennsylvania, Philadelphia, Pennsylvania 19104-6323

Received November 2, 1992

Abstract: Tetrakis(2,4,6-trimethylphenyl)porphyrinato)rhodium(II) ((TMP)Rh) and tetrakis(2,4,6-triisopropylphenyl)-porphyrinato)rhodium(II) ((TTiPP)Rh) occur as low-spin d^7 complexes with EPR parameters associated with a $(d_{xy})^2(d_{xz,yz})^4(d_{z^2})^1$ ground configuration. (por)Rh^{II} species typically react as metalloradicals with a wide variety of substrates to give diamagnetic products; however, the use of increased porphyrin or substrate steric demands has permitted observation of paramagnetic 1:1 adducts. EPR spectra were used in examining features related to the electronic structure for a series of 1:1 five-coordinate complexes with nitrogen, phosphorus, arsenic, and carbon donor ligands. Each of the five-coordinate species is a low-spin d^7 complex with the unpaired electron occupying a d_{z^2} MO $((d_{xy}d_{xz}d_{yz})^6(d_{z^2})^1$ ground configuration). The ligands form 1:1 adducts that have effective axial symmetry with the exceptions of CO, which has as a bent Rh–CO unit, and ethene, which has a symmetrical π complex structure. Donor atom spin densities are estimated from ligand hyperfine coupling. Rhodium-103 hyperfine coupling is used in evaluating the rhodium $4d_{z^2}$ (0.67) and 5s (0.02) spin density in the ethene π complex, which combined with the total ethene C_{2p} (0.278) and C_{2s} (0.008) spin densities, determined from the ligand hyperfine coupling, accounts for most of the unpaired electron. Estimates of the d_{z^2} to d_{xz} and d_{yz} energy separations for the series of 1:1 complexes illustrate the elevation of d_{z^2} by σ donor ligands and the combined lowering of d_{xz}, d_{yz}, and d_{z^2} elevation by ligands with π acceptor ability. Adduct formation of (por)Rh• with π acceptor ligands results in substantially larger d orbital energy separations and ligand spin densities than the strictly σ donor ammine ligands. The d orbital energy separations and ligand spin densities of (por)Rh•L complexes are significantly greater than those observed for the corresponding (por)Co•L complexes, which is also reflected in the greatly enhanced scope of reactivity manifested by (por)Rh• species compared with the analogous Co(II) derivatives. Unusual structural and reactivity properties of the (por)Rh•CO and (por)Rh•C_2H_4 complexes are briefly discussed and contrasted with those of the corresponding (por)Co•L complexes.

Introduction

Cobalt(II) porphyrins and complexes with donor molecules are invariably monomeric low-spin d^7 ($s = {}^1/_2$) species.[1-3] EPR and NMR contact shift studies have been effectively used in probing the electronic structure of the four coordinate (por)Co^{II} species and the perturbations associated with the interaction of donor molecules.[3] Most rhodium(II) complexes including the porphyrin derivatives occur as diamagnetic Rh–Rh-bonded species.[4] Incorporation of sterically demanding substituents on the periphery of the porphyrin ligand has recently been used to block the Rh–Rh bonding and provide a source of four-coordinate low-spin ($s = {}^1/_2$) monomeric rhodium(II) complexes.[5]

Rhodium(II) porphyrins interact with ligands to form complexes, which often react further to produce diamagnetic products.[5-9] Ligand-induced disproportionation of rhodium(II),[6] reductive coupling of CO[5,7] and alkenes,[8] and cleavage of R–OP-$(OR)_2$ bonds[9] illustrate the diversity of reactions manifested by (por)Rh^{II} species. A major aspect of this study has been to use substituent effects on either the ligand or porphyrin to retard or eliminate reactions other than complex formation. This general approach has permitted observation of a series of low-spin d^7 ($s = {}^1/_2$) complexes of (por)Rh• species with diverse classes of ligands in low-temperature (90 K) hydrocarbon frozen solutions. This article describes the use of EPR to examine the electronic structure of (por)Rh^{II}• species and complexes with representative σ donor and π acceptor ligands as a means of gaining insight into the role of complex formation on both the metal center disproportionation and ligand reduction reactions.

Results and Analysis

Analysis of the EPR Parameters for Complexes with a $(d_{xy})^2(d_{xz})^2(d_{yz})^2(d_{z^2})^1$ Ground Configuration. Contributions to the g and A values for the seven-electron (three-hole) case from mixing of excited states into the ground state ($^2A_1$) have been addressed by both Lin[2] and McGarvey.[1] The complete treatment by Lin involves diagonalization of the spin–orbit interaction matrix for the ground and 15 excited states to give the "exact" solution in terms of state energies and the spin–orbit coupling constant. Unfortunately, the resulting expressions contain many more parameters than there are observables such that the equations cannot be uniquely solved. McGarvey's third-order perturbation treatment focuses on the excited states that provide the dominant contributions and uses only the $^2A_1$ ($(d_{xy})^2(d_{xz,yz})^4(d_{z^2})^1$) ground state, one excited doublet state (^2E; $(d_{xy})^2(d_{xz,yz})^3(d_{z^2})^2$), and two

(1) McGarvey, B. R. *Can. J. Chem.* **1975**, *53*, 2498.
(2) Lin, W. C. *Inorg. Chem.* **1976**, *15*, 114.
(3) (a) LaMar, G. N.; Walker, F. A. *J. Am. Chem. Soc.* **1973**, *95*, 1790. (b) Wayland, B. B.; Minkiewicz, J. V.; Abd-Elmageed, M. E. *J. Am. Chem. Soc.* **1974**, *96*, 2795. (c) Walker, F. A. *J. Am. Chem. Soc.* **1970**, *92*, 4235. (d) Wayland, B. B.; Abd-Elmageed, M. E. *J. Am. Chem. Soc.* **1974**, *96*, 4809. (e) Assour, J. M. *J. Chem. Phys.* **1965**, *43*, 2477.
(4) (a) Felthouse, T. R. *Prog. Inorg. Chem.* **1982**, *29*, 73. (b) Boyar, E. B.; Robinson, S. D. *Coord. Chem. Rev.* **1983**, *50*, 109. (c) Wayland, B. B.; Newman, A. R. *J. Am. Chem. Soc.* **1979**, *101*, 6472.
(5) (a) Sherry, A. E.; Wayland, B. B. *J. Am. Chem. Soc.* **1989**, *111*, 5010. (b) Wayland, B. B.; Sherry, A. E.; Poszmik, G.; Bunn, A. G. *J. Am. Chem. Soc.* **1992**, *114*, 1673.
(6) Wayland, B. B.; Balkus, K. J., Jr.; Farnos, M. D. *Organometallics* **1989**, *8*, 950.
(7) (a) Coffin, V. L.; Brennen, W.; Wayland, B. B. *J. Am. Chem. Soc.* **1988**, *110*, 6063. (b) Wayland, B. B.; Sherry, A. E.; Coffin, V. L. *J. Chem. Soc., Chem. Commun.* **1989**, 662.
(8) (a) Bunn, A. G.; Wayland, B. B. *J. Am. Chem. Soc.* **1992**, *114*, 6917. (b) Wayland, B. B.; Poszmik, G.; Fryd, M. *Organometallics* **1992**, *11*, 3534.
(9) Wayland, B. B.; Woods, B. A. *J. Chem. Soc., Chem. Commun.* **1981**, 475.

0002-7863/93/1515-7675$04.00/0

Table I. EPR Parameters for 1:1 Complexes of (por)Rh^{II}· and (por)Co^{II}· in Toluene Glass (90 K)

						$A(^{103}Rh_g)$, MHz			$A(L_g)$, MHz[c]		
complex[a]	g_1	g_2	g_3	C_1 (xz)	C_2[b] (yz)	g_1	g_2	g_3	g_1	g_2	g_3
(TTiPP)Rh·$^{13}C_2H_4$	2.323	2.222	1.982	0.0567	0.0381	72.5	~65	102	<±5	<±5	37.9
(TTiPP)Rh·^{13}CO[d]	2.167	2.138	2.000	0.0287	0.0236			65	318	347	305
(TMP)Rh·^{13}CO[d]	2.176	2.147	1.995	0.029	0.024			67	307	330	299
(TMP)Rh·CNR[e]	2.158		1.995	0.0267				56			28
(TMP)Rh·$AsPh_3$	2.187		2.000	0.0317				85	1023		1150
(TMP)Rh·PPh_3	2.171		2.000	0.0289				60	864		999
(TMP)Rh·PEt_3	2.116		2.004	0.0188				39	948		1154
(TMP)Rh·NC_5H_5[f]	2.300		1.989	0.0524				86			80
(TMP)Rh·$NHEt_2$[f]	2.300		1.992	0.0524				89			86
(TMP)Rh·$NC_5H_3(CH_3)_2$	2.357		1.974	0.0631				104			70
(TMP)Rh·NEt_3	2.390		1.970	0.0694				112			59

						$A(^{59}Co)$, MHz		$A(L_g)$, MHz	
complex[a]	g_1	g_2	g_3	C_1 (xz)	C_2[b] (yz)	$g_\perp$	$g_\parallel$	$g_\perp$	$g_\parallel$
(TMP)Co·^{13}CO	2.237		2.023	0.0363		114	221	163	178
(TPP)Co·^{13}CO[g]	2.217		2.017	0.0339		102	219	166	179
(TPP)Co·$CNCH_3$[g]	2.247		2.025	0.0377		112	201		
(TMP)Co·PEt_3	2.243		2.022	0.0375		100	202	595	685
(TPP)Co·PEt_3[g]	2.243		2.020	0.0379		84	188	528	657
(TPP)Co·$P(OCH_3)_3$[g]	2.244		2.024	0.0374		84	207	828	885
(TMP)Co·PPh_3	~2.31		2.015	(~0.05)			256		524
(TMP)Co·$NHEt_2$	2.32		2.018	(~0.05)			262		37
(TPP)Co·NC_5H_5[h]	2.324		2.027	0.0508		39	237		43

[a] TPP, TMP, and TTiPP are the abbreviations for the tetraphenylporphyrinato, tetrakis(2,4,6-trimethylphenyl)porphyrinato, and tetrakis(2,4,6-triisopropylphenyl)porphyrinato ligands, respectively. [b] Derived from the observed g values and eqs 1–3. $C_1 = \lambda(N_{xz})/\Delta E_{z^2\leftarrow xz}$; $C_2 = \lambda(N_{yz})/\Delta E_{z^2\leftarrow yz}$; $N_{xz(yz)}$ equals the fractional $d_{xz(yz)}$ population in the occupied $d\pi$ molecular orbitals. [c] $A(L)$ is the donor atom electron nuclear coupling constant (L = ^{14}N, ^{31}P, ^{75}As, ^{13}C). [d] The point group symmetries for (TMP)RhCO and (TTiPP)RhCO are probably C_1, and the symmetry restrictions for atomic orbital mixing are removed so that the definition of d_{xz} and d_{yz} is only effective. [e] CNR is 2,6-xylyl isocyanide. [f] Methylcyclohexane glass. [g] Reference 3d. [h] Reference 3c.

quartet states (^{4}E; $(d_{xy})^2(d_{xz,yz})^3(d_{z^2})^1(d_{x^2,y^2})^1$ and $^4A_2$; $(d_{xy})^1(d_{xz,yz})^4(d_{z^2})^1(d_{x^2,y^2})^1$) that arise from singly excited configurations. This approach assumes that states that arise from doubly excited configurations do not significantly contribute for donor adducts of (por)Co^{II}, and Lin's more complete treatment supports this simplification.[2] In both approaches the deviation of $g_\perp$ from 2.0023 for strong donor complexes of (por)Co^{II} species is dominated by intermixing of the ^{2}E into the ground state $^2A_1$ by spin–orbit coupling, and the calculated energy separations for $^2A_1 \leftarrow {}^2E$ ($d_{z^2} \leftarrow d_{xz,yz}$) estimated for 1:1 complexes by the two models are comparable. Four-coordinate (por)M^{II} (M = Co, Rh) species and five-coordinate adducts with weak donors require inclusion of doubly excited configurations and in particular the $^4B_2$ to accommodate $g_\parallel$ values that are substantially less than g_e.[2]

g Value Analysis. The EPR g values for five-coordinate complexes of Co(II) and Rh(II) which have effective axial symmetry have been interpreted by application of McGarvey's third-order perturbation analysis, which includes contributions from the ^{2}E (C_1), ^{4}E (C_3), and $^4A_2$ (C_5) (eq 1 and 2).[1] In these

$$g_\parallel = 2.0023 - 3C_1^2 + 2C_3^2 \quad (1)$$

$$g_\perp = 2.0023 + 6C_1 - 6C_1^2 + (2/3)C_3^2 + (8/3)C_5^2 - (4/3)C_3C_5 \quad (2)$$

expressions $C_1 = \lambda N_1/\Delta E^2_{A_1\leftarrow E}$, where λ is the effective spin–orbit coupling constant ($\rho(d_{z^2})\lambda_0$), N_1 is the fractional contribution of the $d_{xz,yz}$ orbitals to the occupied $d\pi$ molecular orbitals, and $\Delta E^2_{A_1\leftarrow E}$ is the energy separation between the ground ($^2A_1$) and excited (^{2}E) states. $\Delta E^2_{A_1\leftarrow E}$ is commonly designated as $\Delta E_{z^2\leftarrow xz,yz}$ because the $^2A_1$ and ^{2}E states arise from electron configurations where there is single occupancy of the d_{z^2} and $d_{xz,yz}$ orbitals, respectively. The terms from quartet states are similarly defined ($C_3 = \lambda/\Delta E^2_{A_1\leftarrow {}^4E}$; $C_5 = \lambda/\Delta E^2_{A_1\leftarrow {}^4A_2}$).

The cobalt(II) complexes ((por)Co^{II}·L) have observable values for $g_\parallel$ that slightly exceed g_e (g_e = 2.0023) (Table I), which result from the ^{4}E excited state ($C_3 = \lambda/\Delta E^2_{A_1\leftarrow {}^4E}$). Both the ^{4}E ($C_3$) and $^4A_2$ (C_5) contribute to the expression for $g_\perp$, but the complete analysis by Lin[2] illustrates that the ^{4}E and $^4A_2$ are close in energy such that $C_3 \sim C_5$ and the $g_\perp$ expression can be approximated by eq 3. Solving eqs 1 and 3 for C_1 and C_3 results in the values

$$g_\perp \cong 2.0023 + 6C_1 - 6C_1^2 + 2C_3^2 \quad (3)$$

presented in Table I. The Co(II) complexes have $C_3^2 \sim 0.010$–0.015, which places the quartet states $\sim 5 \times 10^3$ cm^{-1} above the ground state. Observation that $g_\parallel \leq g_e$ illustrates that contributions from the ^{4}E and $^4A_2$ quartet states for the (por)Rh^{II} complexes are much smaller than for (por)Co^{II} species because of larger d orbital separations, larger covalency, and reduced interelectronic repulsions. The weakest donors (Et_3N, 2,6-lutidine) form (por)Rh^{II}·B complexes where $g_\parallel$ is slightly smaller than can be accounted for by second-order theory indicate contributions from the $^4B_2$ state.[2]

Complexes of (por)Rh^{II}· with C_2H_4 and CO have low symmetry, and the appropriate g value expressions to second order are given by eqs 4–6.[1]

$$g_{xx} = 2.0023 + 6C_1 - 6C_1^2 \quad (4)$$

$$g_{yy} = 2.0023 + 6C_2 - 6C_2^2 \quad (5)$$

$$g_{zz} = 2.0023 - (3/2)C_1^2 - (3/2)C_2^2 \quad (6)$$

Estimation of the $^2A_1 \leftarrow {}^2E$ ($d_{z^2} \leftarrow d_{xz,yz}$) energy separation from values of λ/C_1 ($\Delta E_{z^2\leftarrow xz,yz}/N_1$) is strictly valid only for complexes with σ donor ligands where $N_1 = 1$. Complexes of π acceptor ligands provide values for the ratio $(\Delta E_{z^2\leftarrow xz,yz})/N_1$. Both increases in $\Delta E_{z^2\leftarrow xz,yz}$ by lowering the $d\pi$ MO and decreases in the $d_{xz,yz}$ contribution to the occupied $d\pi$ orbitals contribute to increasing the λ/C_1 values in complexes where $d\pi \rightarrow p\pi$ back-bonding is important.

^{59}Co and ^{103}Rh Hyperfine Coupling Analysis. The expressions that relate the metal hyperfine coupling constants ($A(^{59}Co)$,

Table II. Derived Spin Densities and d Orbital Energy Separations for (por)M·L (M = Rh, Co)[a] Complexes

complex	$\rho(L_{ns})$	$\rho(L_{np})$	$\rho(L)$	$\sim\rho(D)$	$\sim\rho(Rh_{4d_{z^2}})$	$\rho(Rh_{5s})$	$\sim\lambda$	$\lambda/C_1\,(xz)$	$\lambda/C_2{}^b\,(yz)$
(TTiPP)Rh·$^{13}C_2H_4$	0.008	0.278	0.29	0.30	0.67	0.02	820	14.4	21.4
(TTiPP)Rh·^{13}CO	0.104	>0.20	>0.30	>0.38	<0.60	(0.02)	<730	<25.5	<31.0
(TMP)Rh·PEt_3	0.100	0.239	0.34	0.38	0.60	(0.02)	730	38.8	
(TMP)Rh·$AsPh_3$	0.111	0.166	0.28	0.35	0.63	(0.02)	770	24.2	
(TMP)Rh·PPh_3	0.089	0.158	0.25	0.31	0.67	(0.02)	820	28.3	
(TMP)Rh·NC_5H_5	0.046	0.092	0.14	0.15	0.83	(0.02)	1010	19.3	
(TMP)Rh·$NHEt_2$	0.047	0.141	0.19	0.21	0.77	(0.02)	940	17.9	
(TMP)Rh·$NC_5H_3(CH_3)_2$	0.040	0.081	0.12	0.13	0.85	(0.02)	1040	16.4	
(TMP)Rh·NEt_3	0.032	0.097	0.13	0.14	0.84	(0.02)	1020	14.8	

complex	$\rho(L_{ns})$	$\rho(L_{np})$	$\rho(L)$	$\sim\rho(D)$	$\rho(Co_{3d_{z^2}})$	$\rho(Co_{4s})$	$\sim\lambda$	$\lambda(C_1\,(xz)$	$\lambda/C_2{}^b\,(yz)$
(TMP)Co·CO	0.054	0.055	0.11	0.13	0.82	0.03	420	11.6	
(TPP)Co·$CNCH_3$[c]					0.77	0.03	390	10.5	
(TMP)Co·PEt_3	0.061	0.105	0.17	0.19	0.74	0.03	380	10.2	
(TPP)Co·$P(OCH_3)_3$[c]	0.083	0.066	0.15	0.17	0.71	0.03	370	9.8	
(TPP)Co·(NC_5H_5)[d]	0.025	0.050	0.07	0.08	0.80	0.04	410	8.0	
(TPP)Co·PEt_3[c]	0.056	0.150	0.21	0.23	0.71	0.03	360	9.6	

[a] $\rho(Rh_{4d_{z^2}})$ and $\rho(Co_{3d_{z^2}})$ are the estimated metal d_{z^2} spin densities. $\rho(L)$ is the total donor atom (^{14}N, ^{31}P, ^{75}As, ^{13}C) spin density, and $\rho(D)$ is the estimated total ligand spin density. The methodologies and assumptions used in estimating the ligand and metal spin densities are given in the results section. [b] The values listed for λ/C_1 and λ/C_2 are the upper limiting values for $\Delta E_{z^2\leftarrow xz(yz)}$ in units of KK. The actual values for $\Delta E_{z^2\leftarrow xz(yx)}$ should be reduced by the fractional population of d_{xz}, d_{yz} in the highest occupied $d\pi$ molecular orbitals for the complex. [c] Reference 3d. [d] Reference 3c.

$A(^{103}Rh)$) to the Fermi contact (K), dipolar (P) ($P = g_e\beta_e g_n\beta_n\langle r^{-3}\rangle_{nd}$), and C_1 terms to second order are given by eqs 7 and 8.[1] Values for C_1 obtained by solving the g value expressions

$$A(g_\perp) \cong K + P(4/7 - (6/7)C_1 + (30/14)C_1{}^2) \quad (7)$$

$$A(g_\parallel) \cong K + P(-2/7 + (45/7)C_1 - (57/14)C_1{}^2) \quad (8)$$

are used in evaluating eqs 7 and 8 for P and K. Both the P and λ values for the Co(II) and Rh(II) complexes are assumed to scale linearly with the metal d_{z^2} spin density, $\rho(d_{z^2})$, $(P/P_0 = \lambda/\lambda_0 = \rho(d_{z^2})$, where P_0 and λ_0 are the free ion values (P_0(Co(II)) = 689 MHz;[10,11] λ_0(Co(II)) = 515 cm^{-1};[12] P_0(Rh(II)) = −95.9 MHz;[13] λ_0(Rh(II)) = 1220 cm^{-1}).[13]

The A value expressions required for species which lack a 3-fold or higher symmetry axis are given by eqs 9–11.

$$A(g_{xx}) = K + P(-2/7 + (45/7)C_1 - (57/14)C_1{}^2) \quad (9)$$

$$A(g_{yy}) = K + P(-2/7 + (45/7)C_2 - (57/14)C_2{}^2) \quad (10)$$

$$A(g_{zz}) = K + P(4/7 - (6/14)C_1 - (6/14)C_2 + (15/14)C_1{}^2 + (15/14)C_2{}^2) \quad (11)$$

Ligand Nuclear Hyperfine Coupling. EPR parameters for frozen toluene solutions of (por)Rh• and (por)Co• in the presence of a series of σ donors (NEt_3, $NHEt_2$, NC_5H_5, $NC_5H_3(CH_3)_2$) and ligands with π acceptor capability (PEt_3, PPh_3, $AsPh_3$, CNR, $^{13}C_2H_4$, ^{13}CO) are given in Tables I and II and illustrated in Figures 1 and 2. Ligand nucler hyperfine splittings on the g_3 transition demonstrate that 1:1 complexes are formed with each of these ligands. The 1:1 complexes of (por)Rh^{II}• with NEt_3, $NHEt_2$, NC_5H_5, $NC_5H_3(CH_3)_2$, PEt_3, PPh_3, $AsPh_3$, and CNR and all of the (por)Co^{II}·L complexes have effective axial symmetry (Table I, Figures 1A and 2A) such that $g_1(g_{xx}) = g_2(g_{yy}) = g_\perp$, $g_3(g_{zz}) = g_\parallel$, and $\Delta E_{z^2\leftarrow xz} = \Delta E_{z^2\leftarrow yz} = \Delta E$. For these cases the ligand hyperfine splitting on $g_3(g_{zz})$ is required to be the principal value $A(L)_{zz}$ which permits estimation of the donor atom spin densities. The relationship between the observed ligand hyperfine coupling constants $A(L)$ and the isotropic $\langle A(L)\rangle$ and anisotropic $B(L)$ contributions is given by eqs 12 and 13. For the donor

$$A(L)_{zz} = \langle A(L)\rangle + 2B(L) \quad (12)$$

$$A(L)_{xx} = A(L)_{yy} = \langle A(L)\rangle - B(L) \quad (13)$$

nuclei studied (^{14}N, ^{13}C, ^{31}P, ^{75}As) $\langle A(L)\rangle$ and $B(L)$ have the same sign so that $A(L)_{zz}$ must be larger than $A(L)_{xx,yy}$, which conforms with the experimental observations (Table I). The spin densities for the ligand donor atom s and p orbitals are estimated from the isotropic coupling constant ($\langle A(L)\rangle$), together with the atomic value for the ns orbital ($A_0(ns)$), eq 14, and the anisotropic coupling term $B(L)$ in conjunction with the atomic value for the np orbital ($B_0(np)$), eq 15.

$$\rho_{ns} \cong \langle A(L)\rangle / A_0(ns) \quad (14)$$

$$\rho_{np} \cong B(L)/B_0(np) \quad (15)$$

EPR Studies or Rhodium(II) Porphyrin Complexes. Tetrakis((2,4,6-trimethylphenyl)porphyrinato)rhodium(II), (TMP)Rh•, and tetrakis((2,4,6-triisopropylphenyl)porphyrinato)rhodium(II), (TTiPP)Rh•, have sufficiently large ligand steric requirements that they occur as monomeric low-spin ($S = {}^1/_2$) d^7 complexes.[5] EPR parameters for (TMP)Rh• ($g_1 = g_2 = 2.65$; $g_3 = 1.915$; $C_1 \sim 0.123$; $A(^{103}Rh_{g_3}) = 158$ MHz) and (TTiPP)Rh• ($g_1 = g_2 = 2.823$; $g_3 = 1.852$; $C_1 \sim 0.164$) in toluene glass (90 K) establish that the odd electron is in a relatively localized rhodium d_{z^2} MO associated with a $(d_{xy})^2(d_{xz,yz})^4(d_{z^2})^1$ ground configuration.[1] Hyperfine coupling of the porphyrin pyrrole ^{14}N donor atoms is not directly observed in the EPR of (por)Rh• or any of the 1:1 ligand complexes. Several of the five-coordinate ligand complexes have sufficiently narrow g_3 (g_z) transitions that an upper limit of ~5 MHz can be established for $A(^{14}N_{g_3})$, which translates into a maximum ^{14}N spin density of ~0.01–0.015 per nitrogen of the porphyrin ligand.[14] ^{1}H NMR contact shifts relative to the diamagnetic Zn complex for the pyrrole hydrogens of (TMP)Rh• and (TTiPP)Rh• (~9.6 ppm, T = 295 K) manifest

(10) Abragam, A.; Pryce, M. H. L. *Proc. R. Soc., Ser. A* **1951**, *205*, 135.
(11) McGarvey, B. R. *J. Phys. Chem.* **1967**, *71*, 51.
(12) Dunn, T. M. *Trans. Faraday Soc.* **1961**, *57*, 1441.
(13) Maki, A. H.; Edelstein, N.; Davison, A.; Holm, R. H. *J. Am. Chem. Soc.* **1964**, *86*, 4580.

(14) (a) $A(^{14}N_{g_1}) = \langle A\rangle - (B) < 5$ MHz. $A = \rho(N_{2s})(1540$ MHz); $B = \rho(N_{2p})(47.8$ MHz); $\rho(N_{2p}) \sim 2\rho(N_{2s})$. $A(^{14}N_{g_1}) = \rho(N_{2s})(1540) - \rho(N_{2p})(47.8)$. $A(^{14}N_{g_1}) \sim \rho(N_{2s})(1540 - 95.6) \sim \rho(N_{2s})(1444)$. $A(^{14}N) < 5$ MHz, $\therefore \rho(N_{2s}) < 0.0035$; $\rho(N_{2p}) < 0.0070$; $\rho(N) < 0.0105$; $4\rho(N) < 0.04$. (b) Atomic parameters ($A(L)$, $B(L)$) for the ligand nuclei are taken from a compilation by Drago (Drago, R. S. *Physical Methods for Chemists*, 2nd ed.; Saunders College Publishing: 1992). ^{13}C: $A_0(^{13}C_{2s}) = 3110$ MHz; $B_0(^{13}C_{2p}) = 90.8$ MHz. ^{14}N: $A_0(^{14}N_{2s}) = 1540$ MHz; $B_0(^{14}N_{2p}) = 47.8$ MHz. ^{31}P: $A_0(^{31}P_{3s}) = 10\,178$ MHz; $B_0(^{31}P_{3p}) = 287$ MHz. ^{75}As: $A_0(^{75}As_{4s}) = 9582$; $B_0(^{75}As_{4p}) = 255$ MHz.

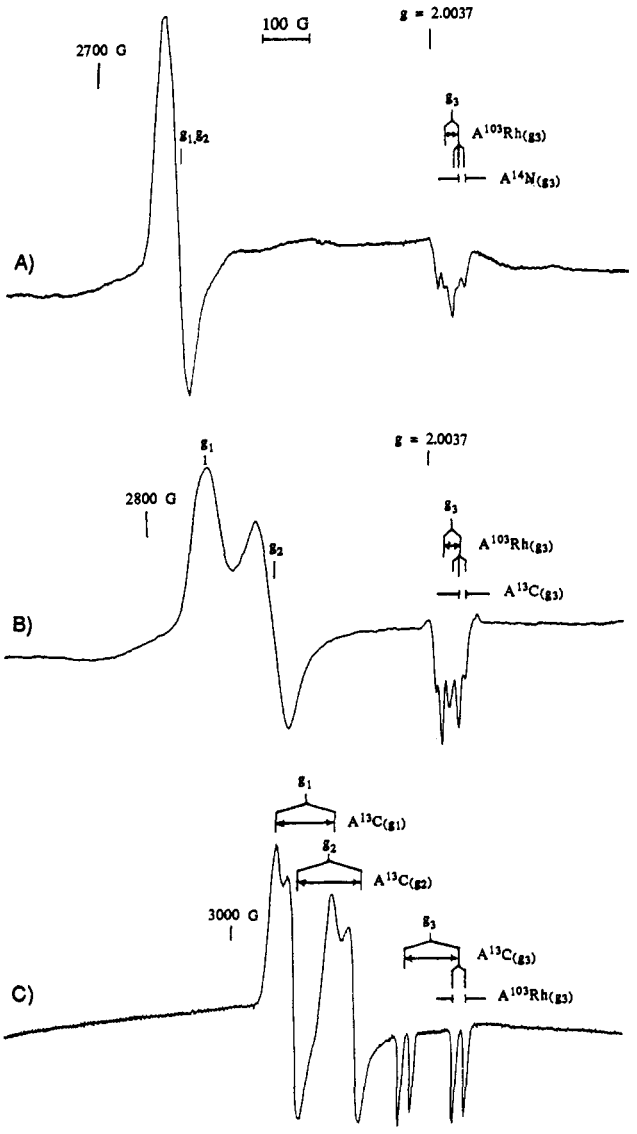

Figure 1. EPR spectra for (por)Rh·L in toluene glass (90 K); ν = 9.520 GHz, sweep width = 1200 G. (A) (TMP)Rh·NEt$_3$; $g_1 = g_2 = 2.39$, $g_3 = 1.970$, $A(^{103}Rh_{g_3}) = 112$ MHz, $A(^{14}N_{g_3}) = 59$ MHz. (B) (TTiPP)Rh·$^{13}C_2H_4$; $g_1 = 2.323$, $g_2 = 2.222$, $g_3 = 1.982$, $A(^{103}Rh_{g_1}) \cong 72.5$ MHz, $A(^{103}Rh_{g_2}) \sim 65.0$ MHz, $A(^{103}Rh_{g_3}) = 102.4$ MHz, $A(^{13}C_{g_1}) \sim A(^{13}C_{g_2}) < 5$ MHz, $A(^{13}C_{g_3}) = 37.9$ MHz. (C) (TTiPP)Rh·^{13}CO; $g_1 = 2.167$, $g_2 = 2.138$, $g_3 = 2.000$, $A(^{103}Rh_{g_3}) = 65$ MHz. $A(^{13}C_{g_1}) = 318$ MHz, $A(^{13}C_{g_2}) = 347$ MHz, $A(^{13}C_{g_3}) = 305$ MHz.

Curie behavior displaying an inverse temperature dependence. A slope of 3.34 ppm K for (TTiPP)Rh• corresponds to an isotropic ^{1}H coupling constant $\langle A^1H \rangle \sim +0.35$ MHz, which illustrates that small positive spin density occurs in the σ donor molecular orbitals of the porphyrin (ρ(H(pyr)) $\sim 1.5 \times 10^{-5}$; 8ρ(H(pyr)) $\sim 1.2 \times 10^{-4}$). The $d_{x^2-y^2}$ is the primary metal d orbital used in σ bonding with the porphyrin donor orbitals, and extensive intermixing is experimentally illustrated by the large ^{14}N hyperfine splitting and nitrogen spin densities observed for d^9 metal porphyrin complexes ((TPP)Cu (4ρ(N) $\sim$ 0.28);[15] (TPP)Ag (4ρ(N) $\sim$ 0.44)[15]) where the unpaired electron resides in the $d_{x^2-y^2}$ orbital. In contrast with the $d_{x^2-y^2}$, the d_{z^2} is only very slightly intermixed with the porphyrin donor orbitals, and the porphyrin ligand spin density is ignored in establishing a model for allocating the spin density and estimating $\Delta E_{z^2 \leftarrow xz,yz}$ for Rh(II) and Co(II) porphyrin complexes. The relative $^2A_1 \leftarrow {}^2E(d_{z^2} \leftarrow d_{xz,yz})$ energy separations for (por)Rh• species are estimated from λ/C_1 (Table I) ($\lambda_{(por)Rh^\bullet} \sim \lambda_{0\ Rh(II)} = 1220$ cm^{-1} [13] and $\lambda_{(por)Rh\cdot L} \sim (\rho(Rh_{d_{z^2}}))\lambda_{0\ Rh(II)}$). (TMP)Rh• in toluene glass has $C_1 = 0.123$ and $\Delta E_{z^2 \leftarrow xy,yz} \sim 9.8 \times 10^3$ cm^{-1}, but in methylcyclohexane glass ($g_\perp \sim 3.0$; $C_1 \sim 0.211$) $\Delta E_{z^2 \leftarrow xz,yz}$ is reduced to 5.8×10^3 cm^{-1}. Toluene clearly perturbs (TMP)Rh• by increasing the d_{z^2} to $d_{xz,yz}$ energy separation, which substantially reduces the $g_\perp$ value. (TTiPP)Rh• has a larger $g_\perp$ ($g_\perp = 2.82$; $C_1 = 0.164$) and smaller ΔE ($\Delta E_{z^2 \leftarrow xz,yz} \sim 7.4 \times 10^3$ cm^{-1}) in toluene glass than (TMP)Rh• ($g_\perp = 2.65$; $C_1 = 0.123$; $\Delta E_{z^2 \leftarrow xz,yz} \sim 9.8 \times 10^3$ cm^{-1}), which may result from steric restrictions on the toluene interactions with the complex.

(TTiPP)Rh·C_2H_4. (TMP)Rh• reacts with ethene to form a two carbon alkyl bridged complex[8a] (TMP)RhCH$_2$CH$_2$Rh(TMP). Increasing the porphyrin steric requirement to the tetrakis(triethylphenyl) derivative, (TTEPP)Rh•, inhibits formation of the two carbon bridged species, but ethene coupling occurs to produce a four carbon bridged complex, (TTEPP)Rh(CH$_2$)$_4$Rh(TTEPP).[8a] Efforts to detect paramagnetic intermediate ethene–metalloradical complexes for these systems were unsuccessful, but further increasing the porphyrin sterics to the tetrakis(triisopropylphenyl) derivative, (TTiPP)Rh•, inhibits ethene coupling, and reversible ethene complex formation is observed at low temperatures ($p_{C_2H_4} \sim 0.3$ atm, $T < 220$ K).

Exposing a toluene solution of (TTiPP)Rh• to $^{13}C_2H_4$ (0.3 atm) and freezing (90 K) results in the EPR spectra shown in Figure 1B and the EPR parameters in Table I. The g_{zz} transition of the $^{13}C_2H_4$ derivative occurs as a doublet of triplets arising from nuclear hyperfine coupling with ^{103}Rh ($A(^{103}Rh_{g_{zz}}) = 102.4 \pm 1.0$ MHz) and two equivalent ^{13}C ($A(^{13}C_{g_{zz}}) = 37.9$ MHz) nuclei in ethene, which identifies the species as a 1:1 ethene π complex. The second-derivative EPR spectrum of (TTiPP)Rh·C_2H_4 displays ^{103}Rh hyperfine splitting on all three g transitions (Table I). The observed g values are used in evaluating eqs 4–6 for C_1 ($\lambda/\Delta E_1$) and C_2 ($\lambda/\Delta E_2$), which are subsequently used with the ^{103}Rh coupling constants in evaluating eqs 9–11 for P and K. Physically plausible parameters result only when $A(^{103}Rh_{g_1,g_2,g_3})$ are all negative because the negative magnetic moment for ^{103}Rh requires P to be negative. This procedure results in the following parameters for (TTiPP)Rh·C_2H_4: $C_1 = 0.0567$; $C_2 = 0.0381$; $P = -63.9 \pm 6$ MHz; $K = -68.1 \pm 6$ MHz. The ratio of P to P_0 yields estimates of the rhodium d spin density ($\rho(Rh_{d_{z^2}}) = P/P_0 = -63.9/-95.9 = 0.67$) and the effective spin–orbit coupling constant ($\lambda = P/P_0(\lambda_0) \sim 817$ cm^{-1}; $P_0(Rh^{II}) = -95.9$ MHz[13] and $\lambda_0(Rh^{II}) = 1220$ cm^{-1} [13], where $P_0(Rh^{II})$ and $\lambda_0(Rh^{II})$ are the free ion values for Rh^{II}. The contact term (K) has contributions from spin polarization of the occupied s orbitals by the 4d spin density ($A(^{103}Rh_{\rho(4d)}) = \rho(4d)(96$ MHz)) and 5s spin density ($A(^{103}Rh_{\rho(5s)}) = \rho(5s)(-6 \times 10^3$ MHz)).[16] Using $K = -68$ MHz and $\rho(4d) = 0.67$ results in an estimate of 0.02 for the rhodium 5s spin density ($\rho(5s) \sim -132$ MHz/-6×10^3 MHz = 0.02). Estimating the d orbital energy separations from the C_1 and C_2 values by using $\lambda \sim 817$ cm^{-1} results in $\Delta E_{z^2 \leftarrow xz}/N_{xz} \sim 14.4 \times 10^3$ cm^{-1} and $\Delta E_{z^2 \leftarrow yz}/N_{yz} \sim 21.4 \times 10^3$ cm^{-1}.

The coordinate system for the ethene complex is based on C_{2v} symmetry, where the z axis is the C_2 axis normal to the porphyrin plane and bisecting the ethene carbons, and the yz plane is defined to contain the Rh, two ethene carbons, and two pyrrole nitrogens such that the d_{yz} is the primary metal dπ donor orbital. Observation of equivalent ethene carbon atoms requires the presence of a 2-fold axis of symmetry, which further requires that this axis (z axis) be a principal direction for both the $\mathbf{g}$ and $\mathbf{A}(^{13}C)$ tensors. The g_1 and g_2 transitions for (TTiPP)Rh• complexes of $^{12}C_2H_4$ and $^{13}C_2H_4$ are virtually superimposable, and thus $\langle A \rangle - B$ is $\sim 0 \pm 5$ MHz. In this situation the ^{13}C coupling constants ($A_{zz}(^{13}C) = 37.9$ MHz; $\langle A(^{13}C) \rangle \sim A_{zz}(^{13}C)/3 \sim 12.6$ MHz) provide estimates for the C_{2p} (0.139), C_{2s} (0.004),

(15) Manoharan, P. T.; Rogers, M. T. In *The Electron Spin Resonance of Metal Complexes*; Yen, T. F., Ed.; Plenum: New York, 1969; pp 143–173.

(16) Muniz, R. P. A.; Vugman, N. V.; Danon, J. *J. Chem. Phys.* **1971**, *54*, 1284.

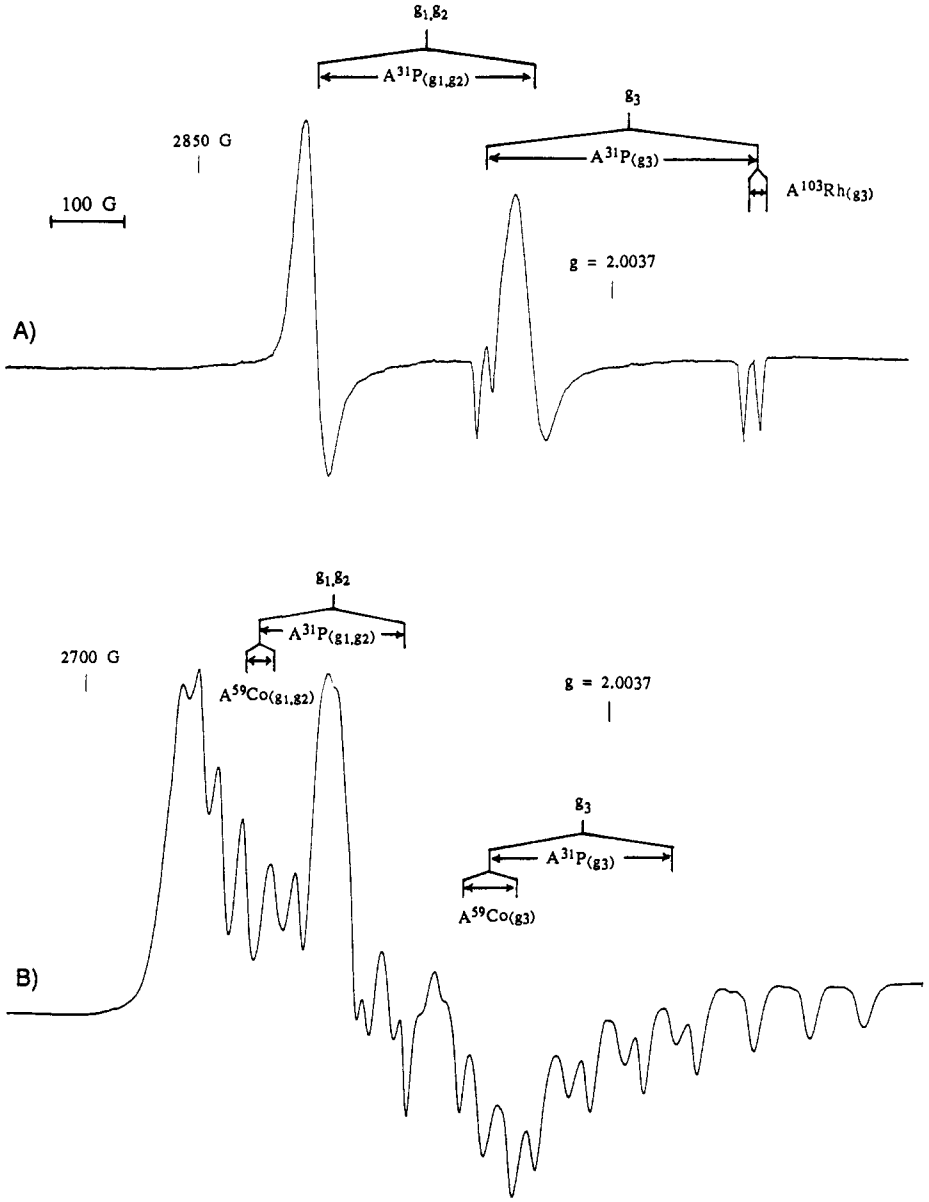

Figure 2. EPR spectra for (por)M·PR_3 in toluene glass (90 K); ν = 9.520 GHz, sweep width = 1200 G. (A) (TMP)Rh·PPh_3; $g_1 = g_2 = 2.17$, $g_3 = 2.000$, $A(^{103}Rh_{g_3}) = 60$ MHz, $A(^{31}P_{g_1,g_2}) = 864$ MHz, $A(^{31}P_{g_3}) = 999$ MHz. (B) (TMP)Co·PEt_3; $g_1 = g_2 = 2.243$, $g_3 = 2.022$, $A(^{59}Co_{g_1,g_2}) = 100$ MHz, $A(^{59}Co_{g_3}) = 202$ MHz, $A(^{31}P_{g_1,g_2}) = 595$ MHz, $A(^{31}P_{g_3}) = 685$ MHz.

and total ethene carbon (0.286) spin densities through evaluation of the following relationships (eqs 12, 14, and 15): $A(^{13}C_{zz}) = \langle A(^{13}C)\rangle + 2B(^{13}C)$; $\langle A(^{13}C)\rangle/3110$ MHz = $\rho(C_{2_s})$; $B(^{13}C)/90.8$ MHz = $\rho(C_{2_p})$).[14b] The spin densities estimated for the rhodium ($\rho(Rh_{4d_{z^2}}) \sim 0.67$; $\rho(Rh_{5_s}) \sim 0.02$) and ethene carbon ($2\rho(C_{2_p}) \sim 0.28$; $2\rho(C_{2_s}) \sim 0.01$) account for most of the unpaired electron density (~0.98) in (TTiPP)Rh·C_2H_4.

Cobalt(II) porphyrins when exposed to C_2H_4 showed no evidence for complex formation even in toluene glass (90 K).

(TMP)Rh·NEt_3. Toluene solutions of (TMP)Rh$^\bullet$ react reversibly with NEt_3 to form a 1:1 complex. The $g_\parallel$ (g_3) transition of (TMP)Rh·NEt_3 is split by ^{103}Rh ($A(^{103}Rh_\parallel) = 112$ MHz and ^{14}N of NEt_3 ($A(^{14}N_\parallel) = 59$ MHz), Figure 1A. Hyperfine coupling is not resolved on the $g_\perp$ transition, which prohibits determination of the rhodium and axial ligand nitrogen spin densities without further assumptions. An estimate of 0.13 for the NEt_3 nitrogen spin density is obtained by using $A(^{14}N_\parallel)$ (59 MHz) and assuming that the donor orbital is an sp^3 hybrid ($\rho(N_{2_p}) = 3\rho(N_{2_s})$). $A(^{14}N_\parallel) = \langle A\rangle + 2B = A_0(^{14}N_{2s})\rho(N_{2_s}) + 2B_0(^{14}N_{2_p})\rho(N_{2_p}) = A_0(^{14}N_{2_s})\rho(N_{2_s}) + 6B_0(^{14}N_{2_p})\rho(N_{2_s})$; $A_0(^{14}N_{2_s}) = 1540$ MHz;[14b] $B_0(^{14}N_{2_p}) = 47.8$ MHz;[14b] $A(^{10}N_\parallel) \sim 1827\ \rho(N_{2_s})$; $\rho(N_{2_s}) \sim 59/1827 = 0.032$; $\rho(N_{2_p}) \sim 3\rho(N_{2_s}) = 0.097$; $\rho(N) \sim 0.13$). The total ligand spin density is estimated as ~0.14 ($\rho(N)/0.9$), and the rhodium 5s spin density ($\rho(Rh_{5_s})$) is estimated at ~0.02.[17] Assuming negligible spin density on the porphyrin results in an estimate of ~0.84 for the rhodium d_{z^2} spin density and $\lambda \sim 1020$ cm^{-1} ($\lambda \sim 0.84\lambda_0$; $\lambda_0 = 1220$ cm^{-1}). Using $C_1 = 0.0694$ and $\lambda \sim 1020$ cm^{-1} gives an estimate of 14.8×10^3 cm^{-1} for $\Delta E_{z^2 \leftarrow xz,yz}$.

(TMP)Rh·$NHEt_2$. $NHEt_2$ reacts with (TMP)Rh$^\bullet$ in toluene at room temperature to form diamagnetic products; however, exposing a precooled (195 K) methylcyclohexane solution of (TMP)Rh$^\bullet$ to $NHEt_2$ vapor and rapidly freezing to 90 K results in observation of the EPR spectrum for a 1:1 complex.

Using the observed $A(^{14}N_\parallel)$ of 86 MHz in (TMP)Rh·$NHEt_2$ and assuming sp^3 hybridization for the ammine nitrogen yields

(17) The spin density on the 4s orbital of cobalt can be calculated for a large number of (por)Co·L complexes studied, as shown in the text, and has been found to be almost independent of L at ~0.03. In the case of (por)Rh·L, a larger percentage of the spin density is transferred from the metal to the ligand, so an even smaller spin density is expected on the 5s orbital of the rhodium. The $\rho(Rh_{5_s})$ can be directly calculated in only one of the complexes studied, (TTiPP)Rh·$^{13}C_2H_4$, and a value of 0.02 was obtained. By analogy to the (por)Co·L complexes, $\rho(Rh_{5_s})$ is expected to be relatively independent of L in (por)Rh·L complexes and is estimated as $\rho(Rh_{5_s})$ ~0.02.

estimates of $\rho(N_{2s}) \sim 0.047$, $\rho(N_{2p}) \sim 0.141$, $\rho(N) \sim 0.19$, and $\rho(NHEt_2) \sim 0.21$. This further yields $\rho(Rh_{d_{z^2}}) \sim 0.77$ and $\lambda \sim 940$ cm^{-1}, which along with C_1 (0.0524) gives $\Delta E_{z^2 \leftarrow xz,yz} \sim 17.9 \times 10^3$ cm^{-1}.

(TMP)Rh·NC$_5$H$_5$ and (TMP)Rh·NC$_5$H$_3$(CH$_3$)$_2$. Addition of an approximately stoichiometric quantity of pyridine to toluene solutions of (TMP)Rh^{II} at 195 K followed immediately by freezing to 90 K produces a new complex with a relatively broad EPR signal centered at $g = 2.0$. The EPR signal disappears and a red precipitate forms if the solution is thawed and then refrozen to 90 K. However, the 1:1 complex of pyridine, (TMP)Rh·NC$_5$H$_5$, is observed in methylcyclohexane glass (90 K). Warming the sample to room temperature and refreezing results in loss of the EPR signal.

Hyperfine coupling from nitrogen is not observed on $g_\perp$ for (TMP)Rh·NC$_5$H$_5$, and an assumed sp^2 hybridization at nitrogen is invoked to obtain estimates of the spin density on the ligand nitrogen. Using the procedures outlined above, the following estimates were obtained: $\rho(N_{2S}) \sim 0.046$, $\rho(N_{2P}) \sim 0.092$, $\rho(N) \sim 0.14$, and $\rho(NC_5H_5) \sim 0.15$. This results in estimates of $\rho(Rh_{d_{z^2}}) \sim 0.83$, $\lambda \sim 1010$ cm^{-1}, and $\Delta E_{z^2 \leftarrow xz,yz} \times 19.3 \times 10^3$ cm^{-1}.

The dimethyl derivative of pyridine, 2,6-lutidine, is a weaker σ donor, and addition to toluene solutions of (TMP)Rh^{II} at 195 K followed by freezing to 90 K results in observation of the 1:1 complex, (TMP)Rh·NC$_5$H$_3$(CH$_3$)$_2$. Hyperfine coupling from nitrogen is observed on $g_\parallel$ ($A(^{14}N_\parallel) = 70$ MHz) but not on $g_\perp$, and estimates of ligand spin densities require the assumption that the nitrogen donor atom is sp^2 hybridized. Using the methodology outlined above, spin densities for the nitrogen donor atom are estimated as $\rho(N_{2s}) \sim 0.040$, $\rho(N_{2p}) \sim 0.081$, $\rho(N) \sim 0.12$, and $\rho(NC_5H_3(CH_3)_2) \sim 0.13$. Allowing for the spin density on the rhodium 5s, $\rho(Rh_{5s}) \sim 0.02$, results in an estimate of $\rho(Rh_{d_{z^2}}) \sim 0.85$, $\lambda \sim 1040$ cm^{-1}, and $\Delta E_{z^2 \leftarrow xz,yz} \sim 16.4 \times 10^3$ cm^{-}

(TMP)Rh·PPh$_3$ and (TMP)Rh·AsPh$_3$. Alkylphosphines and -arsines react rapidly with toluene solutions of (TMP)Rh$^\bullet$ to form diamagnetic products; however, the triphenyl derivatives react reversibly to form 1:1 complexes.

The 1:1 complexes of (TMP)Rh$^\bullet$ with PPh$_3$ and AsPh$_3$ have large hyperfine coupling from ^{31}P and ^{75}As on both the $g_\parallel$ and $g_\perp$ transitions (Figure 2A). ^{31}P and ^{75}As ligand donor atom spin densities of 0.25 and 0.28, respectively, are determined by the following relationships: $A(^{31}P_\parallel) = \langle A \rangle + 2B = A_0(^{31}P_{3s})\rho(P_{3s}) + 2B_0(^{31}P_{3p})\rho(P_{3p})$; $A(^{31}P_\perp) = \langle A \rangle - B = A_0(^{31}P_{3s})\rho(P_{3s}) - B_0(^{31}P_{3p})\rho(P_{3p})$. Evaluating these expressions for $A(^{31}P_\parallel) = 999$ MHz, $A(^{31}P_\perp) = 864$ MHz, $A_0(^{31}P_{3s}) = 10\,178$ MHz,[14b] and $B_0(^{31}P_{3p}) = 287$ MHz[14b] yields $\rho(P_{3s}) \sim 0.089$, $\rho(P_{3p}) \sim 0.158$, and $\rho(P) \sim 0.25$ for (TMP)Rh·PPh$_3$. The donor orbital is estimated to be ~80% phosphorus in character so that $\rho(PPh_3)$ is ~0.31. Evaluating analogous expressions for (TMP)Rh·AsPh$_3$ using $A(^{75}As_\parallel) = 1150$ MHz, $A(^{75}As_\perp) = 1023$ MHz, $A_0(^{75}As_{4s}) = 9582$ MHz,[14b] and $B_0(^{75}As_{4p}) = 255$ MHz[14b] gives $\rho(As_{4s}) \sim 0.111$, $\rho(As_{4p}) \sim 0.166$, and $\rho(^{75}As) \sim 0.28$. Assuming the ligand donor orbital is ~80% arsenic in character gives an estimate of ~0.35 for $\rho(AsPh_3)$.

The rhodium d_{z^2} spin density in (TMP)Rh·PPh$_3$ and λ/λ_0 are thus ~0.67, which, along with $C_1 = 0.0289$, gives an estimate of $\sim 28.3 \times 10^3$ cm^{-1} for $(\Delta E_{z^2 \leftarrow xz,yz})/N_1$. Similarly, the rhodium d_{z^2} spin density and λ/λ_0 for (TMP)Rh·AsPh$_3$ are ~0.63, which combined with $C_1 = 0.0317$ gives $(\Delta E_{z^2 \leftarrow xz,yz})/N_1 \sim 24.2 \times 10^3$ cm^{-1}.

(TMP)Rh·PEt$_3$. Although PEt$_3$ reacts with (TMP)Rh$^\bullet$ to form diamagnetic species, the 1:1 complex can be trapped in toluene glass by immediately freezing the solution upon addition of the ligand. Hyperfine coupling from ^{31}P is observed on both the $g_\parallel$ and $g_\perp$ transitions ($A(^{31}P_\parallel) = 1154$, $A(^{31}P_\perp) = 948$), and spin densities are estimated in the manner outlined above as $\rho(P_{3s}) \sim 0.100$, $\rho(P_{3p}) \sim 0.239$, and $\rho(P) \sim 0.34$. Assuming that the donor orbital of PEt$_3$ is ~90% phosphorus in character yields an estimate of ~0.38 for the total PEt$_3$ spin density. This further provides estimates for the rhodium dz^2 spin density (~0.60), λ (~730 cm^{-1}), and $(\Delta E_{z^2 \leftarrow xz,yz})/N_1$ (~38.8×10^3 cm^{-1}).

(TMP)Rh·CNR (R = 2,6-Dimethylphenyl). Methyl isocyanide rapidly reacts with (TMP)Rh$^\bullet$ to form (TMP)RhCH$_3$ and (TMP)Rh(CN)(RNC); however, 2,6-dimethylphenyl isocyanide forms a transient 1:1 complex that is observed by EPR in toluene glass (90 K).

Both the g and $A(^{103}Rh_\parallel)$ values for (TMP)Rh·CNR are very similar to the PPh$_3$ and AsPh$_3$ complexes. Assuming that the rhodium d_{z^2} spin density and λ/λ_0 values are also comparable (~0.6) and using $C_1 = 0.0267$ provides an estimate of 27×10^3 cm^{-1} for $(\Delta E_{z^2 \leftarrow xz,yz})/N_1$. Using the ^{14}N hyperfine coupling constant of 28 MHz on g_3 and assuming sp hybridization yields an estimate of 0.034 for the isonitrile nitrogen spin density ($\rho(N_{2s}) \sim \rho(N_{2p}) \sim 0.017$; $\rho(N) \sim 0.034$).

(TTiPP)Rh·CO and (TMP)Rh·CO. Toluene solutions of (TMP)Rh$^\bullet$ react with CO ($p_{CO} \sim 1$ atm; $T = 290$ K) to form a dimetal diketone complex, (TMP)RhC(O)C(O)Rh(TMP), resulting from CO reductive coupling.[5a] Although an intermediate mono CO adduct, (TMP)RhCO, has been detected in this system ($g_1 = 2.176$, $g_2 = 2.147$, $g_3 = 1.998$; $A(^{13}C_{g_1}) = 313$, $A(^{13}C_{g_2}) = 325$, $A(^{13}C_{g_3}) = 302$), it is invariably a minority species.[5b] (TTiPP)Rh$^\bullet$ was selected for full investigation because the porphyrin steric demands prohibit CO coupling and provide an equilibrium source for a rhodium(II) mono CO complex (TTiPP)Rh·CO.[5b] The ^{1}H NMR contact shift for the pyrrole porphyrin hydrogens in solutions of (TTiPP)Rh$^\bullet$ with CO ($p_{CO} > 600$ Torr) below 200 K manifests an inverse temperature dependence with a slope of 2.37 ppm K, which we associate with the 1:1 complex (TTiPP)Rh·CO. The ratio of the pyrrole hydrogen hyperfine coupling constants from the ^{1}H contact shifts for (TTiPP)Rh·CO and (TTiPP)Rh$^\bullet$ is 0.70, which reflects transfer of spin density from the $Rh_{d_{z^2}}$ to the CO ligand.

The EPR parameters for (TTiPP)Rh^{13}CO in toluene glass (90 K) are given in Tables I and II and the spectrum illustrated in Figure 1C. Observation of three g value transitions demonstrates that an effective 3-fold or higher axis of symmetry is absent in the CO complex. Large ^{13}C hyperfine splitting is observed on each of the g value transitions ($A(^{13}C_{g_1}) = 318$ MHz, $A(^{13}C_{g_2}) = 347$ MHz, $A(^{13}C_{g_3}) = 305$ MHz), but in contrast with other 1:1 complexes the donor atom nuclear hyperfine splitting is smallest on the g_3 transition, which is also indicative of low symmetry for the CO complex.[5] Deviation of the observed g values from the spin only value is dominated by the rhodium d orbital spin density so that the principal directions of the g tensor are primarily determined by the (por)Rh unit, but the ^{13}C hyperfine tensor has principal directions defined by a local coordinate system centered on carbon. If the principal directions for the g and A(^{13}C) tensors were coincident, then $A(^{13}C_{g_3})$ ($A(^{13}C_{zz}) = \langle A \rangle + 2B$) would be larger than the ^{13}C coupling on the g_1 and g_2 transitions ($A(^{13}C_{xx,yy}) = \langle A \rangle - B$) because both $\langle A \rangle$ and B are positive for ^{13}C.[14b] This condition is fulfilled for all of the 1:1 adducts with the exception of the CO complex (Table I). The pattern of $A(^{13}C)$ values observed on the g value transitions suggests that the complex has C_1 symmetry and that none of the observed ^{13}C splittings correspond to a principal value. In this case the isotropic ^{13}C coupling constant ($\langle A(^{13}C) \rangle = 323$ MHz) gives the C_{2s} spin density ($\rho(C_{2s}) = \langle A(^{13}C) \rangle / 3110$ MHz = 0.10), but only a lower limit for the C_{2p} spin density can be obtained from frozen solution data. The observed ligand nuclear hyperfine splittings have maximum ($\langle A \rangle + 2B$) and minimum ($\langle A \rangle - B$) values as a function of the magnetic field directions ($A(^{13}C) = \langle A(^{13}C) \rangle + B(3\cos^2\theta - 1)$, where θ is the angle between the magnetic field direction and the C_{2p} orbital that contains unpaired electron density). This means that $A(^{13}C_g)$ cannot be less than ($\langle A \rangle - B$) or exceed ($\langle A \rangle + 2B$) and, moreover,

the difference between any two $A(^{13}C_g)$ values cannot exceed $3B$. Using the relationship $\rho(^{13}C_{2p}) = B/90.8$ MHz and the criteria that $A(^{13}C)$ cannot be less than $\langle A(^{13}C)\rangle - B(^{13}C)$ in conjunction with the smallest observed $A(^{13}C)$ ($A(^{13}C_{g_3})$ = 305 MHz) and the isotropic ^{13}C coupling constant ($\langle A(^{13}C)\rangle$ = 323 MHz) gives $B > 18$ MHz and $\rho(C_{2p}) > 0.20$ for the (TTiPP)RhCO complex. The total carbon spin density is greater than 0.30, and the CO carbon orbital containing the odd electron density is at least 67% C_{2p} in character ($C_{2s} < 33\%$). Taking into account the CO oxygen spin density of ~0.08[3b] and the spin density of the Rh_{5s} orbital ($\rho(Rh_{5s}) \sim 0.02$) provides an upper limit of 0.60 for the rhodium d_{z^2} spin density, which further provides an upper limit for λ (~730 cm^{-1}) and upper limits for $(\Delta E_{z^2\leftarrow xz})/N_{xz} \sim 25.5 \times 10^3$ cm^{-1} and $(\Delta E_{z^2\leftarrow yz})/N_{yz} \sim 31.0 \times 10^3$ cm^{-1}.

(TMP)Co·CO. Frozen toluene solutions (90 K) of (TMP)Co• in contact with ^{13}CO (~0.8 atm) produce an EPR spectrum for a 1:1 CO complex (TMP)Co·^{13}CO that has effective axial symmetry, with each ^{59}Co hyperfine component on both the $g_\parallel$ ($g_\parallel$ = 2.023) and $g_\perp$ ($g_\perp$ = 2.237) transitions additionally split into a doublet by one ^{13}C. EPR parameters and derived spin density and d orbital energy separations for (TMP)Co·CO are given in Tables I and II. The g values and cobalt hyperfine coupling on $g_\parallel$ ($A(^{59}Co)_{g_\parallel}$ = +221 MHz) and $g_\perp$ ($A(^{59}Co_{g_\perp}$ = −114 MHz), in conjunction with the cobalt atomic parameters (λ_0 = 515 cm^{-1};[12] P_0 = 689 MHz[10,11]) and eqs 1, 3, 7, and 8, gives values for P (563 MHz), K (−82 MHz), P/P_0 (0.82), $\rho(Co_{d_{z^2}})$ (0.82), λ (420 cm^{-1}), and $(\Delta E_{z^2\leftarrow xz,yz})/N_1$ (11.6×10^3 cm^{-1}). The cobalt 4s spin density ($\rho(4s) \sim 0.033$) is estimated from K = −82 MHz and the relationship $K = \rho(3d)(-252\text{ MHz}) + \rho(4s)(3700\text{ MHz})$.[18] Carbon-13 hyperfine coupling on $g_\parallel$ ($A(^{13}C_{g_\parallel})$ = 178 MHz) and $g_\perp$ ($A(^{13}C_{g_\perp})$ = 163 MHz) yields a C_{2s} spin density of 0.054 ($\rho(C_{2s}) = \langle A(^{13}C)\rangle/(3110\text{ MHz}) = 0.054$), a C_{2p} spin density of 0.055 ($\rho(C_{2p}) = B(^{13}C)/(90.8\text{ MHz}) = 0.055$), and a total carbon spin density of ~0.11. The carbon contributions to the CO donor orbital is ~49% C_{2s}, which is similar to the sp hybrid associated with free CO. The spin density on carbon ($\rho(C) \sim 0.11$) and cobalt ($\rho(3d_{z^2}) \sim 0.82$; $\rho(4s) \sim 0.03$) account for most of the total spin density (~0.96).

(TMP)Co·PEt$_3$. Trialkylphosphines do not react with (TMP)Co• to form diamagnetic species, and the 1:1 complex is observed without the additional complication of 2:1 complex formation (Figure 2B). Hyperfine coupling from phosphorus is observed on both $g_\parallel$ and $g_\perp$ ($A(^{31}P_\parallel)$ = 685, $A(^{31}P_\perp)$ = 595), allowing estimation of spin densities directly from eqs 14 and 15 ($\rho(P_{3s}) \sim 0.061$, $\rho(P_{3p}) \sim 0.105$, $\rho(P) \sim 0.17$, and $\rho(PEt_3) \sim 0.19$). Evaluation of eqs 1, 3, 7, and 8 with the observed $A(^{59}Co)$ and g values yields estimates for P (510 MHz), K (−74 MHz), and P/P_0 ($P/P_0 = 0.74 = \rho(Co_{3d_{z^2}})$; $\rho(Co_{4s}) = 0.030$). This further provides estimates for λ (~380 cm^{-1}) and $(\Delta E_{z^2\leftarrow xz,yz})/N_1$ (~10.2 × 10^3 cm^{-1}).

Discussion

EPR has had only limited application in the study of rhodium(II) complexes[19] because monomeric Rh(II) species usually react to form diamagnetic compounds by Rh–Rh bond formation,[4] disproportionation,[6] and ligand reactions[7-9] (eqs 16–21). Nitrogen donors often induce disproportionation[6] (eq 17), and alkyl isocyanides, phosphites,[9] phosphines, and arsines give X–R bond homolysis (eqs 18 and 19), while unsaturated substrates such as C_2H_4 and CO yield ligand reductive coupling (eqs 20 and 21).[7,8] The primary focus of this study has been to use substituent

$$2(OEP)Rh^\bullet \rightleftharpoons [(OEP)Rh]_2 \quad (16)$$

$$[(OEP)Rh]_2 + 2py \rightleftharpoons (OEP)Rh(py)_2^+ + (OEP)Rh^- \quad (17)$$

$$[(OEP)Rh]_2 + P(OCH_3)_3 \rightleftharpoons (OEP)RhCH_3 + (OEP)RhP(O)(OCH_3)_2 \quad (18)$$

$$(TMP)Rh^\bullet + CH_3NC \rightleftharpoons (TMP)RhCH_3 + (TMP)RhCN \quad (19)$$

$$(TMP)Rh^\bullet + 2CO \rightarrow (TMP)RhC(O)C(O)Rh(TMP) \quad (20)$$

$$(TTEPP)Rh^\bullet + 2C_2H_4 \rightarrow (TTEPP)Rh(CH_2)_4Rh(TTEPP) \quad (21)$$

effects to retard or entirely block reactions of Rh(II) that give diamagnetic products and thus produce a series of low-spin d^7 Rh(II) species where the electronic structure and spin distribution can be probed by EPR spectroscopy. Ligand steric demands associated with (TMP)Rh^{II} and (TTiPP)Rh^{II} prohibit Rh–Rh bonding and produce coordinatively unsaturated planar low-spin d^7 rhodium(II) complexes that give EPR spectra associated with $(d_{xy})^2(d_{xz,yz})^4(d_{z^2})^1$ ground configurations. Disproportionation has been retarded by interacting near stoichiometric amounts of ligand with toluene solutions of (por)Rh• at low temperatures and freezing to trap the adducts. Phenyl derivatives such as 2,6-dimethylphenyl isocyanide, PPh_3, and $AsPh_3$ block the ligand bond rupture, and porphyrin steric effects in (TTiPP)Rh• prohibit CO and C_2H_4 reductive coupling. By manipulating the conditions and utilizing substituent effects, a series of (por)Rh• complexes with ligands was made accessible for study by EPR.

Complexes of (por)Rh• and (por)Co• with σ Donor and π Acceptor Ligands. Interaction of (por)Rh• and (por)Co• complexes with σ donor and π acceptor ligands to form five-coordinate complexes ((por)Rh·L) increases the d_{z^2} to $d_{xz,yz}$ energy separation, intermixes the occupied $d_{xz,yz}$ with ligand π^* orbitals, and transfers spin density from the metal d_{z^2} to the ligand σ molecular orbitals. These electronic effects associated with 1:1 complex formation are manifested in the EPR parameters through decreases in both the observed $g_\perp$ and metal nuclear hyperfine coupling constants ($A(^{103}Rh)$, $A(^{59}Co)$). The observed ligand nuclear hyperfine coupling constants both define the species as 1:1 complexes and provide estimates of the ligand donor orbital spin densities.

1:1 Complexes of NR$_3$, NR$_2$H, NC$_5$H$_5$, NC$_5$H$_3$R$_2$, PX$_3$, AsX$_3$, and CNR. Five-coordinate 1:1 complexes of (TMP)Rh• with NEt_3, $NHEt_2$, NC_5H_5, $NC_5H_3(CH_3)_2$, PEt_3, PPh_3, $AsPh_3$, and CNR and all of the (por)Co• complexes have effective axial symmetry as evidenced by observation of only two g values ($g_\parallel$, $g_\perp$). The ligand nuclei that produce observable coupling (^{14}N, ^{31}P, ^{75}As, ^{13}C) all have positive values for both the isotropic ($\langle A(L)\rangle$) and anisotropic ($B(L)$) contributions to the observed nuclear hyperfine coupling ($A(L)$) so that $A(L_{g_\parallel})$ must be larger than $A(L_{g_\perp})$ ($A(L_{g_\parallel}) = \langle A\rangle + 2B$; $A(L_{g_\perp}) = \langle A\rangle - B$) for an axially symmetric species. Each of these complexes exhibits nuclear hyperfine coupling that is larger on the g_3 ($g_\parallel$) transition than on $g_{1,2}$ ($g_\perp$), which provides further confirmation that these complexes have effective axial symmetry.[5]

Complexes of both σ donor and π acceptor ligands with (por)Rh• have substantially larger $d_{xz,yz}$ to d_{z^2} energy separations than those observed for (por)Co• species (Tables I and II). Ammine σ donor complexes of (por)Rh• exhibit $\Delta E_{z^2\leftarrow xz,yz}$ in the range 14–20 × 10^3 cm^{-1}, while comparable (por)Co• species have $\Delta E_{z^2\leftarrow xz,yz}$ of 7–9 × 10^3 cm^{-1}, and this difference is further magnified in

(18) Symons, M. C. R.; Wilkinson, J. G. *J. Chem. Soc. A* **1971**, *2069*.
(19) (a) Calmotti, S.; Pasini, A. *Inorg. Chim. Acta* **1984**, L 85. (b) Dunbar, K. R.; Haefner, S. C.; Pence, L. E. *J. Am. Chem. Soc.* **1989**, *111*, 5504 and references therein. (c) Billig, E.; Shupack, S. I.; Waters, J. H.; Williams, R.; Gray, H. *J. Am. Chem. Soc.* **1964**, *86*, 926. (d) Bennet, M. A.; Bramley, R.; Longstaff, P. A. *J. Chem. Soc., Chem. Commun.* **1966**, 806. (e) Shock, J. R.; Rogers, M. T. *J. Chem. Phys.* **1975**, *62*, 2640. (f) Hoshino, M.; Yasufuku, K.; Konishi, S.; Imamura, M. *Inorg. Chem.* **1984**, *23*, 1982.

complexes containing ligands with π acceptor capability such as phosphines and isocyanides. Rh(II) porphyrins are both better σ acceptors and more effective $d\pi$ donors than Co(II) porphyrins.

Bonding of ligands on the (por)M z axis places spin density in the ligand σ donor orbital by mixing with the half-occupied d_{z^2}, which is observed in the EPR through ligand nuclear hyperfine splitting. The unpaired electron is confined to the σ molecular orbitals, and thus the ligand nuclear hyperfine couplings only provide information on the σ bonding. Donor atom spin densities in (TMP)Rh·L complexes are substantially larger than those in comparable (por)Co·L species (Table II), which can be ascribed to the larger d orbital radial distribution and corresponding larger d_{z^2}–σ donor orbital overlap associated with 4d compared with 3d orbitals.

Ethene Reactions and Complex Formation with (por)Rh• Species. Rhodium(II) porphyrin complexes with ligand steric requirements of TMP or smaller react with ethene to form two carbon bridged alkyl complexes, (por)$RhCH_2CH_2Rh$(por),[20] and (TTEPP)Rh• produces a four carbon bridged complex, (TTEPP)$Rh(CH_2)_4Rh$(TTEPP).[8a] Increasing the porphyrin sterics to the tetrakis(triisopropylphenyl) derivative, (TTiPP)Rh•, inhibits formation of two and four carbon alkyl bridged complexes, which enables direct observation of reversible ethene complex formation at low temperatures ($p_{C_2H_4} \sim 0.3$ atm, $T < 220$ K). The presence of ^{13}C hyperfine coupling from two equivalent ethene carbons in the toluene glass EPR spectrum of the $^{13}C_2H_4$ adduct demonstrates that the complex has 1:1 stoichiometry, (TTiPP)-Rh·$^{13}C_2H_4$, and further shows on the EPR time scale that the ethene carbons are symmetrically arranged with respect to the Rh(II) center like that in typical π complexes.[21] The π complex structure (C_{2v}) removes the d_{xz}, d_{yz} degeneracy, and thus three g value transitions are observed. The EPR spectrum of (TTiPP)Rh·C_2H_4 is a particularly important example because ^{103}Rh hyperfine coupling is detected on all three g value transitions, which permits the direct evaluation of the $Rh_{4d_{z^2}}$ (0.67) and Rh_{5s} (0.02) spin densities. ^{13}C hyperfine coupling provides estimates of the spin density for each ethene C_{2s} ($\rho(C_{2s}) \sim 0.004 \pm 0.002$) and C_{2p} ($\rho(C_{2p}) \sim 0.14 \pm 0.02$) and the total ethene carbon spin density of ~0.29. Ethene utilizes a virtually pure C_{2p} orbital set $(1/(2^{1/2}))(C_{2p_1} + C_{2p_2})$ in σ bonding with the d_{z^2}. Absence of resolved ethene ^1H hyperfine coupling and the very small C_{2s} character in the odd electron MO indicate that ethene is not significantly rehybridized by bonding with (TTiPP)Rh•. The sum of the $Rh_{4d_{z^2}}$, Rh_{5s}, and ethene carbon spin densities is ~0.98, which accounts for most of the odd electron density and reinforces the conclusion that the porphyrin spin density is negligible. This set of EPR results is important in providing confidence that the rhodium atomic parameters and the approximate procedures for evaluating spin densities from the ^{103}Rh hyperfine coupling constants are reliable.

The π complex structure of (TTiPP)Rh·C_2H_4 (C_{2v} symmetry) removes the $d_{xz,yz}$ degeneracy as manifested by observation of three g value transitions ($(\Delta E_{z^2 \leftarrow xz})/N_{xz} \sim 14.4$ KK; $(\Delta E_{z^2 \leftarrow yz})/N_{yz} \sim 21.4 \times 10^3$ cm^{-1}). The coordinate system for (TTiPP)-Rh·C_2H_4 is defined such that the yz plane contains Rh and the two ethene carbons and two pyrrole nitrogens. The filled d_{yz} is thus the primary $d\pi$ donor orbital that interacts with the ethene $p\pi^*$ and is lowered in energy away from the d_{xz} by $\sim 7 \times 10^3$ cm^{-1}. The occupied d_{xz} is virtually nonbonding so that the $\Delta E_{z^2 \leftarrow xz}$ is an estimate of the elevation of d_{z^2} by the σ interaction with the filled ethene $p\pi$ donor orbital. The d_{z^2} orbital in (TTiPP)Rh• is $\sim 7.4 \times 10^3$ cm^{-1} above the $d_{xz,yz}$ so that the perturbation of ethene binding in (TTiPP)Rh·C_2H_4 raises the d_{z^2} by $\sim 7 \times 10^3$ cm^{-1}, which is equivalent to the lowering of the d_{yz} (7×10^3 cm^{-1}) by the $d\pi$ interaction.

In contrast to the reactivity observed for (por)Rh^{II} species, (por)Co^{II} fails to form an ethene complex in toluene glass (90 K) or produce ethene reduction or coupling, which is a consequence of relatively weak Co–C bonding compared with that of rhodium.[22]

CO Complexes of (por)Rh^{II} and (por)Co^{II}. (TMP)Co• reacts with ^{13}CO to form a complex, (TMP)Co·^{13}CO, which has effective axial symmetry as evidenced by the toluene glass EPR spectrum having only two g transitions ($g_\parallel = 2.023$, $g_\perp = 2.237$) split by ^{59}Co ($I = {}^7/_2$) and a single ^{13}C nucleus. Analysis of the ^{59}Co and g values results in estimates of the Co d_{z^2} spin density ($\rho(Co_{d_{z^2}}) \sim 0.82$) and $\Delta E_{z^2 \leftarrow xz,yz}/N_1$ ($\sim 11.6 \times 10^3$ cm^{-1}). The ^{13}C hyperfine coupling on $g_\parallel$ (g_3) ($A(^{13}C_{g_3}) = 178$ MHz) is larger than on $g_\perp$ (g_1, g_2) ($A(^{13}C_{g_\perp}) = 163$ MHz), which is consistent with effective axial symmetry and corresponds to carbon spin densities of $\rho(C_{2s}) = 0.054$ and $\rho(C_{2p}) = 0.055$ ($\rho(C) \sim 0.11$) and near sp hybridization for the CO donor orbital (~49% C_{2s}). Interaction of CO with (TPP)Co similarly produces a mono CO complex with an effective linear Co–CO unit, moderate d orbital splitting ($\Delta E_{z^2 \leftarrow xz,yy}/N_1 \sim 11.5 \times 10^3$ cm^{-1}), and modest CO carbon spin density ($\rho(C) \sim 0.11$).[3d] These unexceptional properties for (por)Co• species are valuable in emphasizing the currently unique features of (por)RhCO complexes.

Toluene glass EPR spectra for (TMP)Rh·^{13}CO and (TTiPP)-Rh·^{13}CO have three g value transitions with the smallest ^{13}C hyperfine splitting appearing on g_3, which clearly indicates that these CO complexes do not have axial symmetry. The low symmetry is ascribed to a bent Rh–CO unit which reduces the molecular symmetry from C_{4v} to C_s or C_1. If the plane defined by the bent Rh–CO unit is coincident with a plane defined by the (por)Rh unit, then the molecule has a plane of symmetry (C_s), and one of the principal directions of both the **g** and **A**(^{13}C) tensors is required to be normal to the plane. If the Rh–CO plane is rotated with respect to the planes defined by the (por)Rh unit, then the molecular symmetry is C_1, and none of the principal directions are required to be the same for the **g** and **A**(^{13}C) tensors. The pattern of $A(^{13}C)$ values on the g_1, g_2, and g_3 transitions suggests that (por)Rh·CO complexes have C_1 symmetry, where none of the principal directions for the **g** and **A**(^{13}C) tensors are the same. For this lowest symmetry case none of the observed $A(^{13}C_g)$ values for the magnetic field directions defined by g_1, g_2, and g_3 are required to be a principal value for $A(^{13}C)$, and only the isotropic coupling constant $\langle A(^{13}C)\rangle$ (323 MHz) and the minimum value for the anisotropic coupling term $B(^{13}C)$ can be determined from glass EPR spectra. The observed $A(^{13}C_g)$ values are given by the relationship $A(^{13}C) = \langle A(^{13}C)\rangle + B(^{13}C)(3\cos^2\theta - 1)$, where $\langle A(^{13}C)\rangle$ is the isotropic coupling constant (323 MHz) and θ is the angle between the magnetic field and the C_{2p} orbital with spin density. This relationship places upper and lower limits on the observed $A(^{13}C_g)$ of $(\langle A(^{13}C)\rangle + 2B(^{13}C))$ and $\langle A(^{13}C)\rangle - B(^{13}C)$, respectively. Applying these restrictions to the observed $A(^{13}C_g)$ values for (TTiPP)Rh·^{13}CO indicates that the lower limit for $B(^{13}C)$ (18 MHz) is determined by $A(^{13}C_{g_3})$ (305 MHz) and that the C_{2p} spin density must be larger than 0.20 ($\rho(C_{2p}) = B/90.8$ MHz). The isotropic ^{13}C coupling constant gives a C_{2s} spin density of 0.10 ($\rho(C_{2s}) = \langle A(^{13}C)\rangle/3110$ MHz), which combined with a minimum C_{2p} spin density of 0.20 indicates that the total carbon spin density must exceed 0.30. The ratio of the pyrrole hydrogen hyperfine coupling constants for (TTiPP)Rh• and (TTiPP)Rh·CO is 0.70, which is also consistent with a CO spin density of ~0.3. The carbon orbital set used in binding the rhodium d_{z^2} is at least 66% C_{2p} in character, which represents a substantial CO carbon rehybridization (~sp^2) from the ~sp carbon hybridization observed for (TMP)Co·CO.

(20) (a) Ogoshi, H.; Setsune, J.; Yoshida, Z. *J. Am. Chem. Soc.* **1977**, *99*, 3869. (b) Wayland, B. B.; Feng, Y.; Ba, S. *Organometallics* **1989**, *8*, 1438. (c) Sherry, A. E. Ph.D. Dissertation, University of Pennsylvania, 1990. (d) Del Rossi, K. J.; Wayland, B. B. *J. Chem. Soc., Chem. Commun.* **1986**, 1653. (e) Paonessa, R. S.; Thomas, N. C.; Halpern, J. *J. Am. Chem. Soc.* **1985**, *107*, 4333.

(21) (a) Chatt, J.; Duncanson, L. A. *J. Am. Chem. Soc.* **1953**, *75*, 2939. (b) Dewar, M. J. S. *Bull. Soc. Chim. Fr.* **1951**, *18*, C71.

(22) (a) Wayland, B. B. *Polyhedron* **1988**, *7*, 1545. (b) Geno, M. K.; Halpern, J. *J. Am. Chem. Soc.* **1987**, *109*, 1238.

Estimates of the lower limit for the ligand spin densities in (TTiPP)Rh·CO place an upper limit of 0.60 for the rhodium d_{z^2} spin density ($\rho(Rh_{d_{z^2}}) < 0.60$, $\lambda < 730$ cm^{-1}), which also puts upper limits of 25.5 and 31.0 × 10^3 cm^{-1} for $\Delta E_{z^2 \leftarrow xz(yz)}$. The molecular orbitals of (TTiPP)Rh·CO which have their primary origin as the degenerate $d_{xz,yz}$ in (TTiPP)Rh$^{\bullet}$ [8a] are split by ~5 × 10^3 cm^{-1} as a consequence of the bent Rh–CO unit. In contrast, the $d_{xz,yz}$ orbitals in (TMP)Co·CO remain effectively degenerate, and the d_{z^2} to $d_{xz,yz}$ energy separation ($\Delta E_{z^2 \leftarrow xz,yz} \sim 11.6 \times 10^3$ cm^{-1}) is small compared to the rhodium CO complex.

The fundamental differences in the electronic structure and spin distributions for the bent (por)Rh·CO complexes compared to the linear (por)Co·CO are consistent with our observations of acyl radical type reactivity for (por)Rh·CO,[5] which is not mirrored in any way by (por)Co·CO complexes.

Coordination-Assisted and -Induced Reactions of (por)Rh^{II} Complexes. Relatively strong σ donor ligands such as pyridine, diethylamine, and acetonitrile induce disproportionation of (por)Rh^{II} species to form [(por)Rh(L)$_2$]$^+$[(por)Rh]$^-$.[6] The broad transient $g = 2.00$ peak produced from reactions of these ligands with (TMP)Rh$^{\bullet}$ in toluene is tentatively associated with a ligand-induced intramolecular electron transfer from the rhodium center to the porphyrin π^* to form [(por$^{\bullet-}$)Rh^{III}L]. In MO terminology this is equivalent to saying that the d_{z^2} has been elevated above the porphyrin π^* such that the odd electron is transferred to the porphyrin. The intermediate porphyrin anion radical species is viewed as subsequently transferring an electron to a Rh(II) species to give the observed (por)Rh^{III}(L)$_2^+$ and (por)Rh^{I-} disproportionation products.[6] The improved ligand binding with the cationic (por)Rh^{III} compared with (por)Rh$^{II\bullet}$ provides thermodynamic justification for oxidizing the Rh(II) site. Weak donors such as THF and NEt$_3$ do not elevate the d_{z^2} above the porphyrin π^* and are thus ineffective in producing disproportionation and result in persistent complexes of (por)Rh$^{II\bullet}$. Ligands with π acceptor capability such as CO, PPh_3, $CNC_6H_3(CH_3)_2$, and C_2H_4 exclusively form five-coordinate 1:1 complexes with (por)Rh$^{\bullet}$, which fail to produce disproportionation. Apparently the σ donor capability for these ligands is insufficient to elevate the d_{z^2} above the porphyrin π^*, and the large values of λ/C_1 ($\lambda/C_1 = \Delta E_{z^2 \leftarrow xz,yz}/N_1$) must arise primarily from the combined effects of lowering of the $d_{xz,yz}$ and intermixing of the $d_{xz,yz}$ with the ligand π acceptor orbitals associated with $d\pi \rightarrow p\pi$ back-bonding.

(TMP)Rh$^{\bullet}$ reacts with $CNCH_3$ and $P(OCH_3)_3$ to form (TMP)RhCH_3 and (TMP)RhCN or (TMP)RhP(O)$(OCH_3)_2$, respectively. These reactions probably occur through formation of a 1:1 complex with (TMP)Rh$^{\bullet}$ (eqs 22 and 24), which is then probed by a second (TMP)Rh$^{\bullet}$ to find a site for a reaction that produces two stable products in a concerted step (eqs 23 and 25).

$$(TMP)Rh^{\bullet} + CH_3NC \rightleftharpoons (TMP)Rh{\cdot}CNCH_3 \quad (22)$$

$$(TMP)Rh{\cdot}CNCH_3 + {}^{\bullet}Rh(TMP) \rightleftharpoons (TMP)RhCN + H_3CRh(TMP) \quad (23)$$

$$(TMP)Rh^{\bullet} + P(OCH_3)_3 \rightleftharpoons (TMP)Rh{\cdot}P(OCH_3)_3 \quad (24)$$

$$(TMP)Rh{\cdot}P(OCH_3)_2OCH_3 + {}^{\bullet}Rh(TMP) \rightleftharpoons (TMP)RhP(O)(OCH_3)_2 + H_3CRh(TMP) \quad (25)$$

The proposed transition states are envisioned as being trimolecular in a manner similar to that proposed for the reactions of (TMP)Rh$^{\bullet}$ with CH_4[23] and H_2.[24] Substituting phenyl for methyl in the isocyanide and phosphite ligands results in metastable (TMP)Rh·L complexes, where the phenyl group provides a large kinetic barrier to attaining the transition state that results in ligand X–CH_3 bond cleavage.[23]

Carbon monoxide and ethene do not have bonds that are easily cleaved and thus react with (por)Rh^{II} species to give reduction and coupling for the intact ligand unit. Complex formation provides preorganization for subsequent ligand-based radical-like reactions that reduce the substrate (eqs 26–28 and 29–31).

$$(por)Rh^{\bullet} + CO \rightleftharpoons (por)Rh{\cdot}CO \quad (26)$$

$$(por)Rh{\cdot}CO + Rh^{\bullet} \rightleftharpoons (por)RhC(O)Rh(por) \quad (27)$$

$$2(por)Rh{\cdot}CO \rightleftharpoons (por)RhC(O)C(O)Rh(por) \quad (28)$$

$$(por)Rh^{\bullet} + C_2H_4 \rightleftharpoons (por)Rh{\cdot}(C_2H_4) \quad (29)$$

$$(por)Rh{\cdot}(C_2H_4) + {}^{\bullet}Rh(por) \rightleftharpoons (por)Rh(CH_2)_2Rh(por) \quad (30)$$

$$2(por)Rh{\cdot}(C_2H_4) \rightleftharpoons (por)Rh(CH_2)_4Rh(por) \quad (31)$$

Complexes of (por)Rh$^{\bullet}$ with CO and ethene ((por)Rh·CO, (por)Rh·(C_2H_4)) react as sources of ligand-based acyl and alkyl radicals ((por)Rh–CO, (por)Rh$CH_2CH_2^{\bullet}$), and the structures and odd electron distributions in the 1:1 complexes illustrate how adduct formation can guide these radical-like ligand reactions.

Summary

Interaction of ligands with (por)Rh$^{\bullet}$ and (por)Co$^{\bullet}$ results in a series of low-spin ($s = {}^1/_2$) five-coordinate Rh(II) and Co(II) complexes that have $(d_{xy})^2(d_{xz})^2(d_{yz})^2(d_{z^2})^1$ ground MO configurations. The EPR spectrum for (TTiPP)Rh·$^{13}C_2H_4$ provides sufficient observables such that analysis of the EPR parameters yields a relatively complete description of the structure, spin density distribution, and d orbital energy separations ($P = 63.9 \pm 6$ MHz; $K = 68.1 \pm 6$ MHz; $\rho(Rh_{d_{z^2}}) = P/P_0 = 0.67 \pm 0.03$; $\rho(C_{2p}) = 0.139$; $\rho(C_{2s}) = 0.004$; $2\rho(C) = 0.29$; $\lambda = 817$ cm^{-1}; $\Delta E_{z^2 \leftarrow xz} = 14.4 \times 10^3$ cm^{-1}; $\Delta E_{z^2 \leftarrow yz} = 21.4 \times 10^3$ cm^{-1}. The description that emerges for (TTiPP)Rh·$^{13}C_2H_4$ is that of a symmetrically bonded ethene π complex (C_{2v}) where ~30% of the unpaired electron resides on ethene in an orbital that is almost entirely C_{2p} in character. Interaction of (TTiPP)Rh$^{\bullet}$ with the ethene $(2p\pi)\sigma$ donor orbital elevates the d_{z^2} by ~7 × 10^3 cm^{-1}, and the $(2p\pi^*)$ π back-bonding lowers the $d\pi$ donor orbital by ~7 × 10^3 cm^{-1}. Also, the summation of the rhodium ($\rho(Rh) \sim 0.69$) and ethene carbon atom (0.29) spin densities corresponds to ~98% of the odd electron distribution, which provides evidence that the necessarily approximate procedures and atomic parameters used in evaluating the spin densities in other (por)Rh·L complexes are probably reliable for complexes of this type. Although additional assumptions are needed for interpretation of the EPR parameters for 1:1 complexes with ligands other than ethene, consistent trends and comparisons are readily recognizable. Ligands with π acceptor capability produce (por)Rh·L complexes with substantially larger d orbital energy separations and donor atom spin densities than the strictly σ donor ammine ligands. Complex formation of (por)Rh$^{\bullet}$ produces ligand spin densities 1.5–3.0 times greater and d orbital energy separations at least twice that of the corresponding (por)Co·L species. The large perturbations associated with ligand interactions with (por)Rh$^{\bullet}$ are a prelude to metal center disproportionation and ligand reductions that are characteristic of rhodium(II) porphyrin species but not observed for (por)Co^{II} complexes.

(23) Wayland, B. B.; Ba, S.; Sherry, A. E. *J. Am. Chem. Soc.* **1991**, *113*, 5305.

(24) Wayland, B. B.; Ba, S.; Sherry, A. E. *Inorg. Chem.* **1992**, *31*, 148.

Experimental Section

EPR Studies. Electron paramagnetic resonance spectra were obtained by use of an EPR 100 D X-band spectrometer. All g values and hyperfine coupling constants were determined directly from the EPR spectra in conjunction with a diphenylpicryl hydrazide (DPPH) standard as a field calibrant. Additionally, representative spectra were simulated from the experimentally obtained data using Calleo ESR simulation software (version 68881 (2)).[25] Temperature measurements were calibrated with a Bruker Model VT unit using N_2 as the cooling source. Benzene and toluene solvents used in the EPR and NMR studies were first degassed by freeze–pump–thaw cycles and then refluxed over sodium benzophenone until the indicator turned purple. All reagents (ligands, L, for (por)M·(L)) were purchased from Aldrich and were used without further purification. Synthesis of the porphyrins and procedures for the metalation have previously been reported.[5]

(por)M•. Approximately 1 mg of (por)$RhCH_3$ was placed in an EPR tube adapted for vacuum line use. The tube was evacuated, and C_6H_6 was transferred in on the vacuum line. The solution was then irradiated for 6 h ($\lambda \geq 350$ nm) to produce the metalloradical.[5] Benzene was pumped out of the tube to dryness, and h_8-toluene was distilled in, ready for EPR studies. The (por)Co metalloradical can be accessed directly[26] and the dry solid placed directly into an EPR tube adapted for vacuum line use.

Studies of (por)M·(L) for L = CO and C_2H_4. Experimental procedures to study the 1:1 complexes (TMP)Rh·CO, (TTiPP)Rh·CO, and (TTiPP)Rh·C_2H_4 have been reported previously.[5,8a]

Studies of (por)M·(L) for L = PPh_3 and $AsPh_3$. Solid reagents were added in approximately 10-fold excess directly onto the dry metalloradical in an inert atmosphere box (in air, in the case of the Co samples), stoppered, and then evacuated on the vacuum line. Toluene (1 mL) was distilled in on the vacuum line, the solution frozen in liquid nitrogen, and the EPR spectra recorded at a temperature of 90 K.

Studies of (por)M·(L) for L = $NHEt_2$, NEt_3, NC_5H_5, $NC_5H_3(CH_3)_2$, PEt_3 and CNR. The ligand reagents were degassed using freeze–pump–thaw cycles and then vacuum transferred onto precooled (285 K) toluene solutions of the (por)M• metalloradical. The reactants were briefly mixed before freezing in liquid nitrogen to record the EPR spectra. Formation of the 1:1 complex is favored by near stoichiometric addition of the ligand followed by immediate freezing in liquid nitrogen. In the case of the rhodium metalloradicals, formation of the 2:1 complexes is not observed, as this effects further reaction to yield diamagnetic products. The 2:1 complexes are genuine products for the nitrogen donor ligands with (por)Co• metalloradicals and can be accessed free of the 1:1 complex by the addition of a large excess (~20-fold excess) of the ligand followed by slow cooling to 195 K (dry ice/acetone bath) before freezing.

Reaction of (TMP)Rh• with CH_3CN. Addition of acetonitrile, CH_3CN, to toluene solutions of $(TMP)Rh^{II}$ induces disproportionation at the metal center to produce Rh(III) and Rh(I) complexes $[(TMP)Rh(NCCH_3)_2]^+$ and $(TMP)Rh^-$, identified by ^1H NMR and electronic spectra. Product characterization was further verified by independent synthesis of the two complexes. $[(TMP)Rh(NCCH_3)_2]^+CF_3SO_3^-$: (TMP)RhI[5b] (40 mg) and $AgCF_3SO_3$ (10 mg) dissolved in 20 mL of CH_3CN were stirred for 3 h in air at 70 °C. The product, $[(TMP)Rh(NCCH_3)_2]^+CF_3SO_3^-$, was filtered to remove triflate salts, and the product was isolated by removal of the acetonitrile solvent from the filtrate. The complex was then redissolved in benzene for 1 h. ^1H NMR for $[(TMP)Rh(NCCH_3)_2]^+CF_3SO_3^-$ in C_6D_6: 8.92 (s, 8H, pyrrole H), 1.92 (s, 24H, o-CH_3), 7.23 (s, 8H, m-H), 2.49 (s, 12H, p-CH_3), –0.90 (s, 6H, $Rh(NCCH_3)_2$). UV–vis: λ_{max} = 422, 538 nm. The bis-acetonitrile complex can be readily converted to the mono-acetonitrile complex. $(TMP)Rh(NCCH_3)^+CF_3SO_3^-$: Benzene and acetonitrile solvents were removed by rotary evaporation, and fresh benzene was reintroduced. This procedure was repeated until all of the peaks in the proton NMR ascribed to the bis-acetonitrile complex had disappeared. The final product was isolated as an air-stable pink solid. Dissolution of the complex in benzene was very slow, requiring days at room temperature or hours at 80 °C. ^1H NMR for $(TMP)Rh(NCCH_3)^+CF_3SO_3^-$: 9.00 (s, 8H, pyrrole H), 2.04 (s, 12H, o-CH_3), 2.00 (s, 12H, o'-CH_3), 7.22 (s, 4H, m-H), 7.13 (s, 4H, m'-H), 2.46 (s, 12H, p-CH_3), –1.83 (s, 3H, $RhNCCH_3$). FAB MS: 1032 m/e (loss of acetonitrile group; calcd 1074). $(TMP)RhK^+$: 18-crown-6 KOH (20 μL) in 0.5 mL of benzene was added to 1 mg of (TMP)RhH dissolved in the same solvent. The anion formed is only sparingly soluble, $\sim 2 \times 10^{-5}$ M. ^1H NMR in C_6D_6: 8.38 (s, 8H, pyrrole H), 1.62 (s, 12H, o-CH_3), 1.60 (s, 12H, o'-CH_3), 2.38 (s, 12H, p-CH_3), m-H are obscured by the solvent. UV–vis: λ_{max} = 408, 518 nm.

Reaction of (TMP)Rh• with CH_3NC. EPR spectra that result from addition of methyl isocyanide to toluene solutions of $(TMP)Rh^{II}$ at 195 K and refreezing to 90 K are always poorly resolved and transient ($g_\perp \sim 2.12$, $g_\parallel \sim 1.996$; ^{103}Rh and ligand ^{14}N hyperfine coupling are not resolved). ^1H NMR data for these solutions show the equal formation of two major diamagnetic species which are assigned as methyl isocyanide adducts of $(TMP)RhCH_3$ and (TMP)RhCN. $(CH_3NC)(TMP)RhCH_3$: ^1H NMR (δ in C_6D_6) 8.79 (s, 8H, pyrrole H), 7.19 (s, 4H, m-CH_3), 7.09 (s, 4H, m'-CH_3), 2.44 (s, 12H, p-CH_3), 2.14 (s, 12H, o-CH_3), 1.83 (s, 4H, o'-CH_3), –5.79 (d, 3H, $RhCH_3$, $^2J_{RhH}$ = 2.2 Hz). FAB MS: 898 m/e (loss of acetonitrile group; calcd 939). $(CH_3NC)(TMP)RhCN$: ^1H NMR (δ in C_6D_6) 8.90 (s, 8H, pyrrole H), 7.19 (s, 4H, m-CH_3), 7.04 (s, 4H, m'-CH_3), 2.43 (s, 12H, p-CH_3), 2.07 (s, 12H, o-CH_3), 1.86 (s, 12H, o'-CH_3), –0.47 (s, 3H, $RhCNCH_3$). FAB MS: 950 m/e (calcd 950).

Variable Temperature ^1H NMR Studies. Approximately 1 mg of $(TTiPP)RhCH_3$ was placed in an NMR tube adapted for vacuum line use. The tube was evacuated, and C_6H_6 was transferred in on the vacuum line. The solution was then irradiated for 6 h ($\lambda \geq 350$ nm) to produce the metalloradical.[5] Benzene was pumped out of the tube to dryness, d_8-toluene was distilled in, and the tube was flame sealed, ready for ^1H NMR studies. The ^1H NMR spectrum was recorded at various temperatures between 178 and 378 K using a Bruker AF500 instrument with an FTS refrigerator unit, utilizing the boil-off from liquid nitrogen at low temperatures. A plot of chemical shift, δ, against inverse temperature (K), $1/T$, for the pyrrole porphyrin hydrogens is a straight line demonstrating Curie law behavior.

The procedure was repeated with the addition of carbon monoxide (~600 Torr) on the vacuum line to a cooled solution of (TTiPP)Rh• in d_8-toluene prior to sealing the tube. The variable temperature ^1H NMR spectra were recorded in the same manner. The chemical shifts of all peaks differ from those of (TTiPP)Rh• at room temperature due to partial coordination of CO to the metalloradical. Below 200 K the ^1H NMR contact shift for the pyrrole porphyrin hydrogens displays an inverse temperature dependence which is associated with full coordination of CO to the metalloradical to give the 1:1 complex (TTiPP)Rh·CO.

Acknowledgment. The authors would like to acknowledge the support of the National Science Foundation through Grant CHE-90-14923 and the Department of Energy, Division of Chemical Sciences, Office of Basic Energy Sciences, Grant DE-FG02-86ER 13615. We also thank the Science and Engineering Research Council, United Kingdom, for a studentship (to A.G.B.).

(25) *Calleo ESR*, 68881 (2) Version; Calleo Scientific Software Publishers: Fort Collins, CO, 1989.

(26) Rothemund, P.; Menotti, A. R. *J. Am. Chem. Soc.* **1948**, *70*, 1808.